Catalysis Science & Technology

Accepted Manuscript

ROYAL SOCIETY OF CHEMISTRY

www.rsc.org/catalysis

Catalysis Science & Technology

PAPER

Highly active electron-deficient Pd clusters on N-doped active carbon for the hydrogenation of aromatic ring†

Received 00th January 20xx,
Accepted 00th January 20xx

DOI: 10.1039/x0xx00000x

www.rsc.org/

Renfeng Nie*, Hezhan Jiang, Xinhuan Lu, Dan Zhou and Qinghua Xia*

N-doped active carbon (N-AC) has been synthesized *via* a heat treatment of the mixture consisted of dicyandiamide as the nitrogen source and commercial active carbon as the precursor. This material is especially adapted for anchoring ultrafine Pd nanoparticles by a very clean strategy using H_2 as the reductant. The physicochemical properties of materials are investigated by powder X-ray diffraction (XRD), Raman, Fourier transform infrared spectroscopy (FTIR), transmission electron microscopy (TEM) and X-ray photoelectron spectroscopy (XPS). The results reveal that the variation of the treatment temperature can assist the tuning of the content of N and the dispersion of Pd on *x*N-AC, by which Pd nanoparticles with a narrow size distribution centered at around 1.8 nm can be obtained. These robust catalysts show very high catalytic activity in the aromatic ring hydrogenation of acidic substrates, such as electron-deficient benzoic acid or electron-rich phenol, under mild conditions in aqueous media. Excellent catalytic results (9.2 times higher activity in comparison to undoped catalyst for benzoic acid hydrogenation), high stability and easy recyclability of the catalyst are achieved. The strong interaction between pyridinic nitrogen group and Pd species will lower down the reducibility of Pd species and result in the formation of relatively electron-deficient ultra-small sized Pd clusters, thus leading to the high activity in the hydrogenation.

Introduction

Due to their stability, ease of separation and recyclability, heterogeneous catalysts are dominant in chemical industry.[1, 2] In principle, in the case of supported catalysts, two basic but important issues should be taken into account in order to design and screen suitable supports for catalytic applications. The support must be stable, has a high surface area, and should contain rich defect sites. There are many kinds of materials suitable as supports, among which metal oxides,[3] zeolites,[4] and carbons (including activated carbon,[5] carbon nanotubes[6] and graphene[7]) are the most frequently used. The carbon materials are often chosen as candidates due to their high surface areas and low cost. However, the weak interaction of NPs with carbons can lead to aggregation or leaching, which inevitably reduces the catalytic activity. To overcome this limitation, the modification of carbons (oxidized with H_2O_2 or HNO_3) is necessary in most cases.[8] Enormous interests have been focused on the development of efficient and recyclable catalysts with environmentally-benign characteristics.

The transformation of aromatics into value-added chemicals or high-quality fuels is a very important class of reactions.[9, 10] For example, the aromatic ring hydrogenation of benzoic acid (BA) is the most effective method in the synthesis of cyclohexane carboxylic acid (CCA), which is an important organic intermediate for the synthesis of pharmaceuticals like praziquantel and ansatrienin.[11, 12] Usually, the hydrogenation of aromatic ring with electron-withdrawing groups requires more severe conditions than that with electron-donating groups,[13, 14] which will result in the occurrence of some undesired side reactions, such as the hydrogenation of carboxylic groups into alcohols at high temperatures and pressures.[15] Thus, there is a need for the design of the catalyst with a high activity and stability based on economic and environmental considerations.

Nitrogen-containing carbons, as a kind of fascinating materials, have attracted worldwide attention recently.[16-18] It has been reported that N-dopants in the carbon skeleton can be usually regarded as favourable anchoring sites or defects for enhancing the particle nucleation and reducing the particle size.[19-21] At the same time, the N doping results in an improvement in the hydrophilicity and basicity of supports,[22] beneficial to the use of the prepared catalysts in aqueous phase and the sufficient interaction of the acidic substrate with basic support.[23] The introduction of N can modify the electronic structure of the carbon matrix, and strengthen the interaction between carbon and guest molecules due to the

Hubei Collaborative Innovation Center for Advanced Organic Chemical Materials, & Ministry-of-Education Key Laboratory for the Synthesis and Application of Organic Functional Molecules, School of Chemistry and Chemical Engineering, Hubei University, Wuhan 430062, P.R. China.
E-mail: refinenie@163.com (N. R. Nie); xiaqh518@aliyun.com (Q. H. Xia); Fax/Tel: +86 27 88662747

† Electronic Supplementary Information (ESI) available: Additional experimental results. See DOI: 10.1039/x0xx00000x

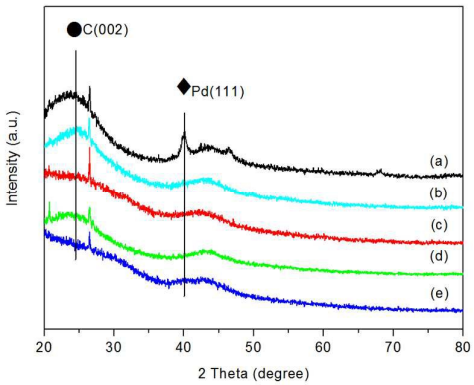

Fig. 1 XRD patterns of (a) Pd/AC, (b) Pd/400N-AC, (c) Pd/600N-AC, (d) Pd/800N-AC and (e) Pd/1000N-AC.

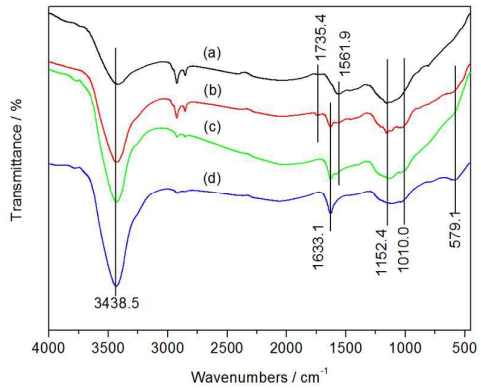

Fig. 3 FTIR spectra of (a) Pd/400N-AC, (b) Pd/600N-AC, (c) Pd/800N-AC and (d) Pd/1000N-AC.

high charge and spin density caused by the nitrogen,[24] which may help lower the activation energy barrier of electron-deficient benzene ring leading to a high hydrogenation rate. To date, many studies have reported the improved catalytic activity of carbon-based catalysts by increasing the metal dispersion initiated by N-doping.[25-29] Moreover, it is found that the nature of N species in nitrogen-doped materials has a profound impact on the electronic structure of metal NPs (e.g., Pd) and their catalytic property.[30, 31]

Herein, we report a simple preparation method for N-doped active carbon (N-AC) supported Pd NPs and its applications in the selective hydrogenation of electron-deficient aromatic ring under mild conditions. The influence of N dopant on the morphology of Pd and the BA hydrogenation are discussed.

Results and discussion

Synthesis and microstructure of highly dispersed Pd nanoparticles over N-AC

The XRD patterns in Fig. 1 show a decrease in C(002) intensity with increasing the treatment temperature, indicating the presence of much more disordered carbon framework derived from the thermal treatment of AC.[32] The very sharp and intense reflections at 21° and 27° are ascribable to the microcrystalline structure of carbon. The pattern (Fig. 1a) of the material prepared without dicyandiamide demonstrates a sharp Pd(111) peak. Upon the N incorporation at different temperatures, the intensity of the Pd peak in Pd/*x*N-AC decreases and becomes faint, indicating the decrease of Pd crystalline size, meaning that N-dopant is a key role in controlling the dispersion of Pd in N-doped carbon materials.

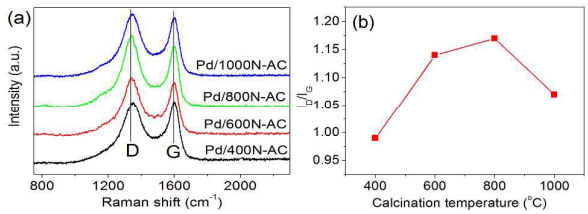

Fig. 2 (a) Raman spectra and (b) I_D /I_G values of Pd/*x*N-AC.

The Raman spectra of the materials prepared at different temperatures are presented in Fig. 2, in which the G band at ~ 1590 cm^{-1} indicates the in-plane vibration of sp2 carbon atoms,[33] while the D band at ~1350 cm^{-1} is a defect-induced Raman feature representing the imperfect crystalline structure of the material.[34] With increasing the temperature from 400 to 800 °C, the I_D/I_G value shows an increase from 0.99 to 1.17. However, a further increase of temperature such as the sample Pd/1000N-AC leads to a decrease of I_D/I_G value. This result indicates the formation of much more structural defects in 800N-AC.

Fig. 3 shows the FT-IR spectra of Pd/*x*N-AC samples treated at different temperatures. The strong band at 3438 cm^{-1} may be related to N–H or O–H stretching vibrations or water molecules.[32] The absorption band at 2900 cm^{-1} is attributed to C-H stretching vibration. The peaks observed at 1570–1634 cm^{-1} correspond to the C=N bond and fluctuate obviously with increasing the temperature, implying the rearrangement of N-functional groups on the surface of *x*N-AC.

The chemical compositions of the N-doped carbon materials were analysed by using both CHNS elemental analysis and XPS photoelectron spectroscopy. As shown in Table S1, reasonable amounts of nitrogen (N) are detected from all N-doped samples, and the surface nitrogen content obtained from the XPS data is from 1.5 to 9.1 at. % (Fig. S1), significantly higher than the bulk nitrogen content from 0.7 to 7.3 at. %, calculated by elemental analysis. This indicates the N species are more enriched on the surface than in the bulk, favourable for its catalytic application. The N-free AC supported Pd shows a surface area of 759 m^2/g with a pore volume of 0.46 cm^3/g (Table S2), which are decreased obviously for Pd/400N-AC, indicating the N precursor blocks the tunnels of AC. As the treatment temperature is increased from 400 to 1000 °C, the BET surface area and pore volume of the samples is increased from 531 to 747 m^2/g and from 0.38 to 0.45 cm^3/g, suggesting that thermal decomposition of N-functional groups leads to the partial recovery of pore structure of AC.

To determine the mean particle sizes of as-synthesized catalysts,

Table 1 Physical properties of N-doped carbon materials.

Catalysts	Particle size (nm)		Relative atomic percentage (%)				Relative atomic percentage (%)	
	XRD	TEM	N (398.5 eV)	N (400.1 eV)	N (401.1 eV)	N (403.3 eV)	Pd^0	$Pd^{\delta+}$
Pd/AC	10.8	12.0	-	-	-	-	78.6	21.4
Pd/400N-AC	n.d	3.4	50.6	47.5	1.9	0	40.3	59.7
Pd/600N-AC	n.d	3.1	51.4	39.8	8.7	0.1	15.5	84.5
Pd/800N-AC	n.d	1.8	58.1	21.3	18.9	1.7	0	100
Pd/1000N-AC	n.d	2.7	42.7	13.5	35.3	8.5	27.7	72.3

the TEM images are obtained (Fig. 4). It is found that the mean particle size of Pd on the undoped AC is 12 nm. When the content of Pd is fixed at 2.5 wt. %, the mean particle size of Pd will be decreased from 3.4 to 1.8 nm with the increase of temperature from 400 (400N-AC) to 800 °C (800N-AC) during the synthesis. The TEM images (Fig. 4d) show the presence of uniformly well-dispersed Pd NPs on very large surfaces of 800N-AC, in which those NPs exhibit no aggregation into large clusters. A high-resolution TEM image for the Pd/800N-AC clearly shows that the distance between two adjacent lattice planes of Pd NPs is approximately 0.225 nm, indicative of a crystalline Pd structure. Much high temperature (1000 °C), however, will lead to a slight increase of the mean size to 2.7 nm (Table 1), in relation to the low N content of support and relatively weak interaction between Pd and the support.

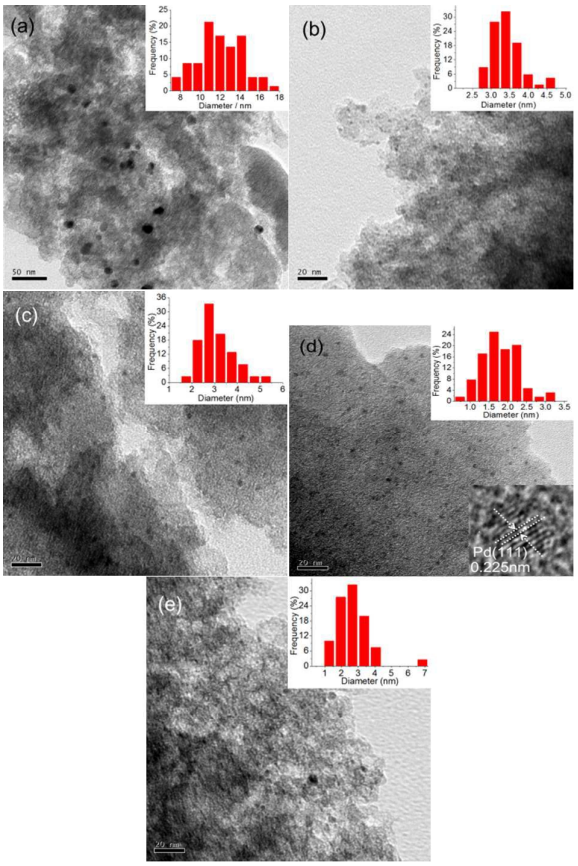

Fig. 4 The TEM images of (a) Pd/AC, (b) Pd/400N-AC, (c) Pd/600N-AC, (d) Pd/800N-AC and (e) Pd/1000N-AC. The insets in images of (a-e) are corresponding histograms of Pd particle size distribution. The inset in image of (d) is high resolution TEM image of Pd nanoparticles in Pd/800N-AC.

The C1s peak of Pd/*x*N-AC (Fig. 5) locates at approximately 284.5 eV with two tail peaks at 283 and 288 eV, assigned to C-Pd bonding[35] and the electron-deficient carbons bound to nitrogen (C-N), respectively. With increasing the treatment temperature, this C-N signal is weakened significantly, along with an enhancement of the peak at 292 eV, suggesting the pyridine-like or aromatic N is partly transformed into graphitic N in carbon skeleton. Too high temperature but makes this signal weakened again.

All of the high-resolution N 1s XPS spectra (Fig. 6) are broad and asymmetric, indicating that several types of binding configurations are related to the involved nitrogen atoms. As for 400N-AC and 600N-AC, the curve deconvolution shows that the N 1s spectra can be separated into several peaks, at 398.5, 400.1, 401.1, and 403.3 eV.[36-39] The lowest-energy peak is assigned to aromatic N atoms that are bonded to two C atoms (C=N-C) in the triazine or heptazine rings. The peak at 400.1 eV is assigned to sp2-hybridized N atoms that are bonded to three C atoms (e.g., C-N(-C)-C). The peaks at high binding energies of 401.1 and 403.3 eV are attributed to sp3-hybridized terminal N atoms (e.g., $-NH_2$) and their charging effects, respectively. As for 800N-AC and 1000N-AC, these nitrides are partially converted and undergo dynamic surface rearrangement during heating. The peaks centered at 398.5, 400.1, 401.1, and 403.3 eV can be attributed to pyridinic nitrogen (N-1), pyrrolic nitrogen (N-2), quaternary nitrogen (N-3), and pyridine oxide-N (N-4), respectively.[40] The contents of four types of nitrogen atoms are listed in Table 1. Noticeably, with the increase of the temperature from 800 to 1000 °C, the proportion of quaternary nitrogen shows an increase from 18.9 to 35.3 %, while that of pyridinic nitrogen (N-1) decreases from 58.1 to 42.7 %, meaning that the re-assembly of surface into graphite cluster during heating will lead to the aromatization with the introduction of a large amount of N into the graphitic structure.[40] However, the resonances N-1 and N-3 are the dominant species, in agreement with the report in the literature.[30]

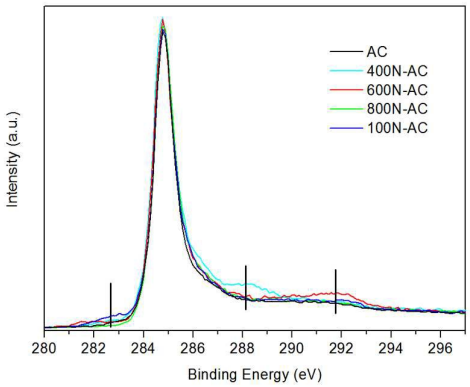

Fig. 5 XPS spectrum of C1s of Pd/*x*N-AC.

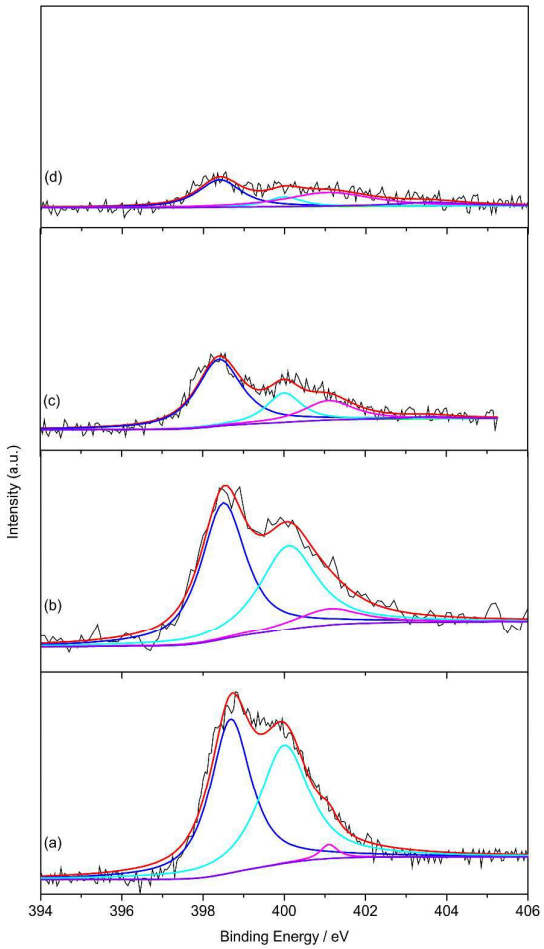

Fig. 6 The N1s spectra of (a) Pd/400N-AC, (b) Pd/600N-AC, (c) Pd/800N-AC and (d) Pd/1000N-AC (from bottom to top).

The Pd^0 $3d_{5/2}$ and $3d_{3/2}$ doublets are observed at 335.6 and 340.9 eV, as shown in Fig. 7. Palladium in the oxidation state is also detected (the doublet pair at 337.7 and 342.9 eV).[41] The presence of $Pd^{\delta+}$ species, characterizing both the deposition of pure and N-doped AC, can be attributed to the oxidation of Pd due to the formation of Pd-O bond by air exposure.[42] Moreover, for the N-doped AC, the percentage of $Pd^{\delta+}$ increases obviously from 21.4 to 100 % with increasing the temperature to 800 °C (Table 1). A further increase of the treatment temperature to 1000 °C leads to the decrease of this value to 72.3 % due to the decrease of N content. It should be considered whether the $Pd^{\delta+}$ fluctuation is caused by a size effect of Pt NPs, namely that the atomic Pd usually has higher BE than bulk Pd.[43] In this work, the size effect is unlikely to be the exclusive origin of BE shift, because the size effect on BE is usually negligible in the size range of 1.8-3.4 nm.[44, 45] Although Pd/600N-AC has much higher $Pd^{\delta+}$ percentage (84.5 %) than Pd/400N-AC (59.7 %), its particle size is close to that of Pd/400N-AC. Moreover, Pd/1000N-AC has a lower $Pd^{\delta+}$ percentage (72.3 %) than Pd/600N-AC (84.5 %), while its particle size is smaller than that of Pd/400N-AC. And, there is no clear relationship between $Pd^{\delta+}$ percentage and Pd size. Therefore, the fluctuation can be attributed to a strong interaction between nitrogen groups and Pd NPs.

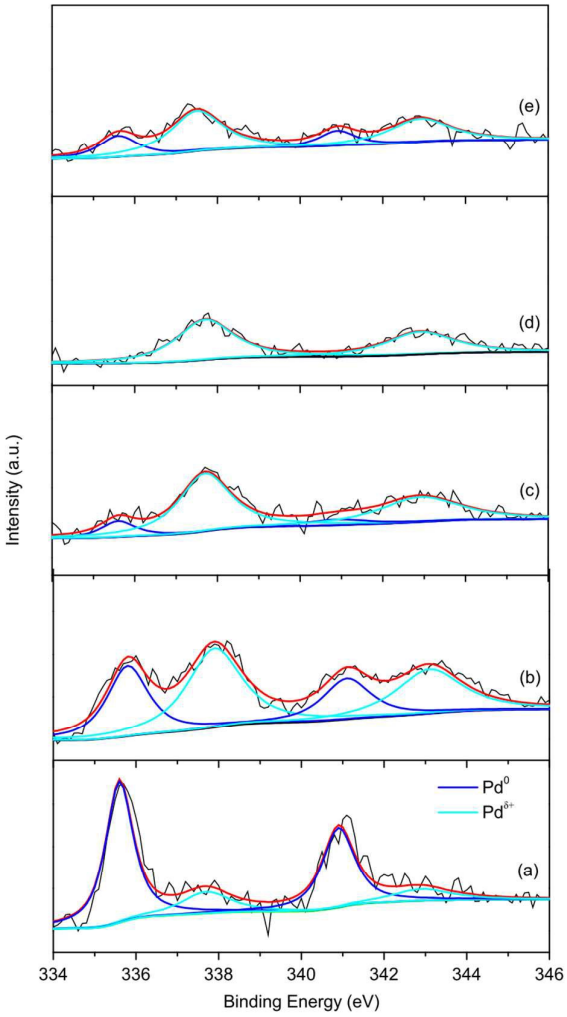

Fig. 7 XPS spectra of Pd3d in (a) Pd/AC, (b) Pd/400N-AC, (c) Pd/600N-AC, (d) Pd/800N-AC and (e) Pd/1000N-AC (from bottom to top).

Previous results in the literature suggested that pyridinic N and quaternary-N sites could facilitate both the coordination of metal ions and the anchoring of metal NPs.[45] XPS spectra showed that pyridinic or aromatic (C=N-C) nitrogen atom existed dominantly in N-AC, which was often associated with defect sites on edges of graphite layers [46] or on vacancy sites.[47] At the same time, Li et al. [48] showed that the interaction of Pt with the carbon system containing quaternary N atoms was weaker than that with the carbon system containing pyridinic N atoms on vacancy sites. Arrigo et al. [30] found that the divalent Pd species were more abundant when Lewis basic sites in the form of pyridine N species were present, which indicated that the coordination at these sites lowered down their reducibility at the reduction conditions used. These results indicate that pyridinic or aromatic (C=N-C) nitrogen atom exerts important impacts on the electronic properties of Pd, thus leading to the high percentage of $Pd^{\delta+}$ species. The thermal treatment at high temperature (up to 1000 °C) leads to the reduction of the pyridine N species, the coordination capacity of the support, and the relative contribution of $Pd^{\delta+}$ on the surface of

1000N-AC. Therefore, the obvious fluctuation in the Pd peak and particle size is likely due to the effect of pyridinic or aromatic (C=N-C) nitrogen in Pd/*x*N-AC.

Table 2 Hydrogenation of benzoic acid over different catalysts.[a]

Entry	Catalysts	t (h)	T (°C)	Yield (%)
1	Pd/AC	2	110	7.2
2	Pd/400N-AC	2	110	43.5
3	Pd/600N-AC	2	110	48.2
4	Pd/800N-AC	2	110	65.9
5	Pd/1000N-AC	2	110	59.3
6[b]	Pd/AC	2	110	24.5
7	Pd/SiO_2	2	110	1.2
8	Pd/Al_2O_3	2	110	0.4

[a] Reaction conditions: 0.5 mmol BA, 20 mg catalyst, 5 mL H_2O, 2.5 MPa H_2.
[b] Purchased from Aladdin company.

Catalytic property of highly dispersed Pd nanoparticles

The hydrogenation of BA to CCA is carried out over Pd/*x*N-AC at 110 °C under 2.5 MPa (Table 2). It is apparent that the N-free catalyst (referred to as Pd/AC, entry 1) shows a poor activity (only 7.2 % conversion) in this transformation. However, all the N-doped AC supported Pd catalysts (Table 2, entries 2-5) exhibit higher activities than the undoped one. With increasing the treatment temperature from 400 to 800 °C, the conversion is increased from 43.5 to 65.9 % over Pd/800N-AC. A further prolongation of reaction time to 3.5 h leads to a conversion of 97.4 % with 100 % selectivity of CCA (Fig. S2). Even in the case of large-scale BA hydrogenation reaction (1.0 g BA, 16-fold scale-up, 0.16 mol % Pd, see Table S3), the reaction can efficiently proceed to afford 92.4 % yield of CCA without any decrease in the performance. Much high treatment temperature, however, results in a slightly reduced activity, e.g. 59.3 % for Pd/1000N-AC (Table 2, entry 5). Other frequently used heterogeneous Pd-based catalysts inclusive of Pd/SiO_2, Pd/Al_2O_3 and commercial Pd/AC (entries 6-8) achieve a poor hydrogenation activity < 25 % under the same reaction conditions. Importantly, the Pd/800N-AC catalyst can be reused several cycles without an obvious loss in its activity (Fig. S3).

It must be noted that the solvent plays a key role in determining the reaction rate or the distribution of products. Among these solvents tested (Table S4), apolar cyclohexane and protic ethanol are unfavourable for the titled reaction (entries 2-4). In aprotic THF

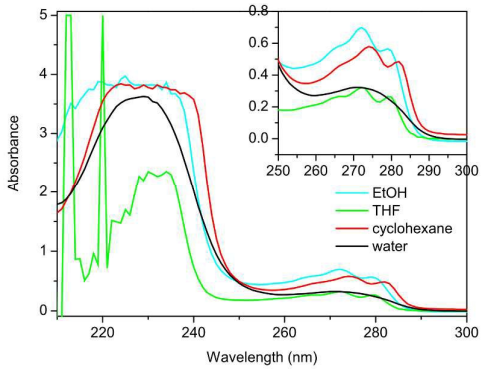

Fig. 8 The UV-vis spectra of BA in different solvents.

Table 3 Hydrogenation of phenol over different catalysts.[a]

Entry	Catalysts	t (h)	Conversion (%)	Selectivity (%)
1	Pd/AC	4	24.8	93.5
2	Pd/400N-AC	4	48.6	98.1
3	Pd/600N-AC	4	53.7	95.1
4	Pd/800N-AC	4	79.4	94.3
5	Pd/1000N-AC	4	67.8	92.2
6	Pd/800N-AC	1	25.6	93.6
7	Pd/800N-AC	6	98.4	93.0

[a] Reaction conditions: 19.6 mg (0.2 mmol) phenol, 20 mg catalyst, 5 mL H_2O, 40 °C, 0.3 MPa H_2。

(entry 2), the BA conversion is only 21.3 %. Although water has the lowest solubility of H_2 than other solvents,[49] it results in the highest conversion of 65.9 % and 100 % selectivity of CCA (entry 1). It is found that the water is the best solvent for BA hydrogenation, and the conversion is significantly decreased with decreasing the polarity of the solvents. The polarity of solvent can markedly affect the BA adsorption behaviour on the surface of Pd/*x*N-AC. In water, the carboxyl group of BA will face toward the solvent, but the aromatic ring will be oriented toward the catalyst, which leads to desired ring hydrogenation. However, low polarity of solvent may lead to much less regular orientation, unbeneficial to the ring hydrogenation.[50] Fig. 8 is the UV-vis spectra of BA in these four solvents. It is found that BA in THF, cyclohexane and ethanol displays three absorption peaks between 260 and 290 nm, corresponding to n-π* transition of –COOH,[50] but only one board absorption peak in water. This change can be reasoning that the strong H-bond donor capability of water towards carboxyl group can help lower down the activation energy barrier and accelerate the hydrogenation rate.

To further demonstrate the versatility of the Pd/*x*AC catalyst, the selective hydrogenation of acidic phenol to cyclohexanone is performed at 40 °C for 4 h under 0.3 MPa H_2 (Table 3). The use of N-free AC as the support leads to an inferior activity in the hydrogenation (entry 1), giving only 24.8 % conversion of phenol and 93.5 % selectivity. However, Pd/400N-AC (entry 2) gives an improved conversion of 48.6 % and selectivity of 98.1 %. Further increasing the treatment temperature (entries 3, 4), the phenol conversion is increased from 48.6 to 79.4 % over Pd/800N-AC, accompanied by a slight reduction of cyclohexanone selectivity from 98.1 to 94.3 %. A further prolongation of reaction time to 6 h leads to a conversion of 98.4 % with 93.0 % selectivity (entry 7). The conversion of phenol reaches a maximum over Pd/800N-AC, and then decreases to 67.8 % over Pd/1000N-AC (entry 5). These results indicate that the content and variation of N dopant have played important roles in the hydrogenation of phenol again.

Clearly, the introduction of N dopant is the key to enhance the catalytic hydrogenation. The N-functionalization of the support leads to strong interactions with the active sites of catalysts.[21, 26, 51] In this work, the surface pyridinic or aromatic (C=N-C) nitrogen species on AC provide the co-interaction sites for Pd species, which gives rise to strong metal–N bond at the interface, further to good dispersion and narrow size distribution of Pd nanoparticles. Those small particles are responsible for the enhanced catalytic performance. Moreover, this dominant pyridinic or aromatic (C=N-

C) nitrogen on the support can serve as Lewis basic sites to increase the hydrophilicity and basicity of *x*N-AC,[22, 39] which may benefit the dispersion of catalyst in water to improve the exposure of the catalyst to the acid substrates (e.g., benzoic acid, phenol), hence accelerating the diffusion and transformation of substrates.

Conclusions

Highly dispersed electron-deficient Pd clusters over *x*N-AC, Pd/*x*N-AC, has been prepared by a clean strategy using H_2 as the reductant. Varying the treatment temperature of the mixture consisted of dicyandiamide and active carbon can assist the tuning of the dispersion of Pd on *x*N-AC, by which Pd nanoparticles with a narrow size distribution centered at around 1.8 nm can be obtained. These robust catalysts show high catalytic activity and excellent reusability in the aromatic ring hydrogenation of acidic substrates, such as electron-deficient benzoic acid or electron-rich phenol, as compared to the commonly used Pd/AC catalyst. The enhanced catalytic performance can be attributed to the intimate interaction of N groups with highly dispersed Pd NPs.

Experimental

Materials

Active carbon (AR) with surface area of 816 m^2/g were purchased from Hunan Xiangda Chemical Reagent Co.. Dicyandiamide (CP, 98 %), benzoic acid (AR, 99.5 %), H_2O_2 (28 %), $PdCl_2$ (AR, Pd >59 %), phenol (AR, 99 %) and other chemicals (analytical grade) were used without further purification.

Preparation of N-doped AC

Ten grams of active carbon (AC) was first immersed in 250 mL H_2O_2 (28 wt. %) solution. The slurry was stirred and treated at 50 ^oC for 5 h. Then the solid was recovered by filtration and washed thoroughly with distilled water. Thus-pretreated AC was dried in a vacuum oven at 80 ^oC for 10 h, which was denoted as H_2O_2-AC. Appropriate amount of dicyandiamide (0.5 g) was added into a suspension of 2.0 g H_2O_2-AC while stirring. The slurry was stirred for 30 min at 60 ^oC and sonicated for 30 min, and then water was removed under reduced pressure at 60 ^oC. The resulting powder was transferred into a crucible, heated to given temperature at a heating rate of 2 $^oC{\cdot}min^{-1}$ under a flow of nitrogen and kept for 4 h. The sample was then cooled down to room temperature under the protection of N_2. The carbon material was denoted as *x*N-AC, where *x* corresponds to the treatment temperature.

Preparation of highly-dispersed Pd nanoparticles over N-AC

One gram of the support was dispersed in water (50 mL), then added with 41.7 mg $PdCl_2$ (2.5 wt. %) while stirring. After 30 min, the reduction treatment was performed in a 100 mL Teflon-lined autoclave at 40 ^oC for 8 h under 2 MPa H_2. Then, the precipitate was recovered by filtration and washed thoroughly with deionized water. The resulting Pd catalyst was dried in oven at 80 ^oC overnight and named as Pd/*x*N-AC. The synthesis of Pd/AC was the same as that of Pd/xN-AC, in which AC was pretreated at 600 ^oC for 4 h under N_2 protection. The real amount of loading Pd was detected via inductively coupled plasma-atomic emission spectroscopy (ICP, Plasma-Spec-II spectrometer).

Characterizations

Powder X-ray diffraction (XRD) was performed on a Bruker D8A25 diffractometer with Cu$K\alpha$ radiation (λ = 1.54184 Å) operating at 30 kV and 25 mA in the range of 5–80^o 2θ. Fourier transform infrared (FTIR) spectra were analyzed on an OPUS Fourier Transform Infrared Spectrophotometer in the range of 400–4000 cm^{-1}. For IR characterizations, a mixture of 3 mg of catalysts powder and 200 mg of potassium bromide (KBr) was pressed into a thin wafer. X-ray photoelectron spectra (XPS) were recorded on a Perkin-Elmer PHI ESCA system. X-ray source was standard Mg anode (1253.6 eV) at 12 kV and 300 W. Transmission electron microscope (TEM) images were obtained using an accelerating voltage of 200 kV on a JEOL-135 2010F Transmission Electron Microscope. Raman spectra were collected at room temperature from 100 to 4000 cm^{-1} with 514.5-nm argon ion laser (Rhenishaw Instruments, England). The spectra were recorded with a resolution of 2 cm^{-1}.

Selective hydrogenation of aromatic ring

The hydrogenation reaction was carried out in a 25 mL stainless autoclave with a Teflon liner. In a typical procedure, a certain amount of catalyst was dispersed in 5 mL solvent, and then added with a required amount of substrate. The autoclave was sealed, purged and pressurized with hydrogen, and then heated to desired temperature under magnetic stirring at a rate of 1000 rpm. After the completion of the reaction, the mixture was separated by extraction and centrifugation in order to remove the water and solid catalyst. The filtrate was analyzed by gas-chromatogram (GC, HP 5890, USA) with a 30 m capillary column (HP-5) using a flame ionization detector (FID). And, all the products were analyzed by GC–MS (Agilent 6890).

Acknowledgements

This work was supported by National Natural Science Foundation of China (21173073, 21273064, 21503074, 21571055), Natural Science Fund for Creative Research Groups of Hubei Province (2014CFA015), Natural Science Fund of Hubei Province (2015CFB232), the Key Project of the Education Department of Hubei Province (D20141004), and the 2014 Sci-tech Support Project of the Science and Technology Department of Hubei Province (2014BAA098). The authors thank Referees and Editor for their valuable suggestions on the revision of the manuscript.

Notes and references

1. P. F. Vogt and J. J. Gerulis, in *Ullmann's Encyclopedia of Industrial Chemistry*, Wiley-VCH Verlag GmbH & Co. KGaA, 2000.
2. R. Rinaldi and F. Schuth, *Energy Environ. Sci.*, 2009, **2**, 610-626.
3. S. F. J. Hackett, R. M. Brydson, M. H. Gass, I. Harvey, A. D. Newman, K. Wilson and A. F. Lee, *Angew. Chem. Int. Ed.*, 2007, **46**, 8593-8596.
4. Q. H. Xia, K. Hidajat and S. Kawi, *J. Catal.*, 2002, **205**, 318-331.

5.J. A. Anderson, A. Athawale, F. E. Imrie, F. M. Mkenna, A. Mcue, D. Molyneux, K. Power, M. Shand and R. P. K. Wells, *J. Catal.*, 2010, **270**, 9-15.
6.J. Wang, G. Fan and F. Li, *Catal. Sci. Technol.*, 2013, **3**, 982-991.
7.R. Nie, J. Wang, L. Wang, Y. Qin, P. Chen and Z. Hou, *Carbon*, 2012, **50**, 586-596.
8.X. Chen, G. Wu, J. Chen, X. Chen, Z. Xie and X. Wang, *J. Am. Chem. Soc.*, 2011, **133**, 3693-3695.
9.D. Bianchi, R. Bortolo, R. Tassinari, M. Ricci and R. Vignola, *Angew. Chem. Int. Ed.*, 2000, **39**, 4321-4323.
10. A. Stanislaus and B. H. Cooper, *Catal. Rev.*, 1994, **36**, 75-123.
11.H. Shinkai, K. Toi, I. Kumashiro, Y. Seto, M. Fukuma, K. Dan and S. Toyoshima, *J. Med. Chem.*, 1988, **31**, 2092-2097.
12. B. S. Moore, H. Cho, R. Casati, E. Kennedy, K. A. Reynolds, U. Mocek, J. M. Beale and H. G. Floss, *J. Am. Chem. Soc.*, 1993, **115**, 5254-5266.
13. P. Zhang, T. Wu, M. Hou, J. Ma, H. Liu, T. Jiang, W. Wang, C. Wu and B. Han, *ChemCatChem*, 2014, **6,** 3323-3327.
14. B. Chen, U. Dingerdissen, J. G. E. Krauter, H. G. J. Lansink Rotgerink, K. Möbus, D. J. Ostgard, P. Panster, T. H. Riermeier, S. Seebald, T. Tacke and H. Trauthwein, *Appl. Catal. A,* 2005, **280**, 17-46.
15. E. J. Grootendorst, R. Pestman, R. M. Koster and V. Ponec, *J. Catal.*, 1994, **148**, 261-269.
16. Z. Zhao, Y. Dai and G. Ge, *Catal. Sci. Technol.*, 2015, **5**, 1548-1557.
17. Z. Wei, Y. Gong, T. Xiong, P. Zhang, H. Li and Y. Wang, *Catal. Sci. Technol.*, 2015, **5**, 397-404.
18. X. Wang, G. Sun, P. Routh, D.-H. Kim, W. Huang and P. Chen, *Chem. Soc. Rev.*, 2014, **43**, 7067-7098.
19. R. Nie, J. Shi, W. Du, W. Ning, Z. Hou and F.-S. Xiao, *J. Mater. Chem. A*, 2013, **1**, 9037-9045.
20. F. Cervantes-Sodi, G. Csányi, S. Piscanec and A. C. Ferrari, *Phys. Rev. B*, 2008, **77**, 165427.
21. G. Vilé, D. Albani, M. Nachtegaal, Z. Chen, D. Dontsova, M. Antonietti, N. López and J. Pérez-Ramírez, *Angew. Chem. Int. Ed.*, 2015, **54**, 11265-11269.
22. Y. Zhou, R. Pasquarelli, T. Holme, J. Berry, D. Ginley and R. O'Hayre, *J. Mater. Chem.*, 2009, **19**, 7830-7838.
23. E. Haque, J. W. Jun, S. N. Talapaneni, A. Vinu and S. H. Jhung, *J. Mater. Chem.*, 2010, **20**, 10801-10803.
24. Y. Gao, G. Hu, J. Zhong, Z. Shi, Y. Zhu, D. S. Su, J. Wang, X. Bao and D. Ma, *Angew. Chem. Int. Ed.*, 2013, **52**, 2109-2113.
25. D. He, Y. Jiang, H. Lv, M. Pan and S. Mu, *Appl. Catal., B*, 2013, **132-133**, 379-388.
26. L. Jia, D. A. Bulushev, O. Y. Podyacheva, A. I. Boronin, L. S. Kibis, E. Y. Gerasimov, S. Beloshapkin, I. A. Seryak, Z. R. Ismagilov and J. R. H. Ross, *J. Catal.*, 2013, **307**, 94-102.
27. P. Zhang, Y. Gong, H. Li, Z. Chen and Y. Wang, *Nat Commun.*, 2013, **4**, 1593.
28. R. Arrigo, M. E. Schuster, S. Wrabetz, F. Girgsdies, J.-P. Tessonnier, G. Centi, S. Perathoner, D. S. Su and R. Schlögl, *ChemSusChem*, 2012, **5**, 577-586.
29. R. Arrigo, S. Wrabetz, M. E. Schuster, D. Wang, A. Villa, D. Rosenthal, F. Girsgdies, G. Weinberg, L. Prati, R. Schlögl and D. S. Su, *Phys. Chem. Chem. Phys.*, 2012, **14**, 10523.
30.R. Arrigo, M. E. Schuster, Z. Xie, Y. Yi, G. Wowsnick, L. L. Sun, K. E. Hermann, M. Friedrich, P. Kast, M. Hävecker, A. Knop-Gericke and R. Schlögl, *ACS Catal.*, 2015, **5**, 2740-2753.
31. R. Arrigo, M. E. Schuster, S. Abate, S. Wrabetz, K. Amakawa, D. Teschner, M. Freni, G. Centi, S. Perathoner and M. Hävecker, *ChemSusChem*, 2014, **7**, 179-194.
32. C. H. Choi, M. W. Chung, H. C. Kwon, S. H. Park and S. I. Woo, *J. Mater. Chem. A*, 2013, **1**, 3694-3699.
33. V. Chandra, J. Park, Y. Chun, J. W. Lee, I.-C. Hwang and K. S. Kim, *ACS Nano*, 2010, **4**, 3979-3986.
34. H. Wang, X. Xiang and F. Li, *J. Mater. Chem.*, 2010, **20**, 3944-3952.
35. G. Deniau, L. Azoulay, P. Jégou, G. Le Chevallier and S. Palacin, *Surf. Sci.*, 2006, **600**, 675-684.
36. J. Xu, T. Chen, Q. Jiang and Y.-X. Li, *Chem. Asian J.*, 2014, **9**, 3269-3277.
37. A. Thomas, A. Fischer, F. Goettmann, M. Antonietti, J.-O. Müller, R. Schlögl and J. M. Carlsson, *J. Mater. Chem.*, 2008, **18**, 4893-4098.
38. Q. Su, J. Sun, J. Wang, Z. Yang, W. Cheng and S. Zhang, *Catal. Sci. Technol.*, 2014, **4**, 1556-1562.
39. A. Thomas, A. Fischer, F. Goettmann, M. Antonietti, J.-O. Müller, R. Schlögl and J. M. Carlsson, *J. Mater. Chem.*, 2008, **18**, 4893-4908.
40. R. Arrigo, M. Hävecker, R. Schlögl and D. S. Su, *Chem. Commun.*, 2008, 4891-4893.
41. X. Chen, F. M. Yasin, P. K. Eggers, R. A. Boulos, X. Duan, R. N. Lamb, K. S. Iyer and C. L. Raston, *RSC Adv.*, 2013, **3**, 3213-3217.
42.W. Ju, M. Favaro, C. Durante, L. Perini, S. Agnoli, O. Schneider, U. Stimming and G. Granozzi, *Electrochim. Acta*, 2014, **141**, 89-101.
43. W. E. Kaden, C. Buchner, L. Lichtenstein, S. Stuckenholz, F. Ringleb, M. Heyde, M. Sterrer, H. J. Freund, L. Giordano, G. Pacchioni, C. J. Nelin, P. S. Bagus, *Phys. Rev. B* 2014, **89**, 115436.
44.J. Zhu, A. Holmen and D. Chen, *ChemCatChem*, 2013, **5**, 378-401.
45. X. Ning, H. Yu, F. Peng and H. Wang, *J. Catal.*, 2015, **325**, 136-144.
46. Y. Zhou, K. Neyerlin, T. S. Olson, S. Pylypenko, J. Bult, H. N. Dinh, T. Gennett, Z. Shao and R. O'Hayre, *Energy Environ. Sci.*, 2010, **3**, 1437-1446.
47. L. Bulusheva, A. Okotrub, A. Kurenya, H. Zhang, H. Zhang, X. Chen and H. Song, *Carbon*, 2011, **49**, 4013-4023.
48. Y.-H. Li, T.-H. Hung and C.-W. Chen, *Carbon*, 2009, 47, 850-855.
49. X. Xu, M. Tang, M. Li, H. Li and Y. Wang, *ACS Catal.*, 2014, **4**, 3132-3135.
50. G. Bai, X. Wen, Z. Zhao, F. Li, H. Dong and M. Qiu, *Ind. Eng. Chem. Res.,* 2013, **52**, 2266-2272.
51. T. He, L. Liu, G. Wu and P. Chen, *J. Mater. Chem. A*, 2015, **3**, 16235-16241.

Graphical Abstract

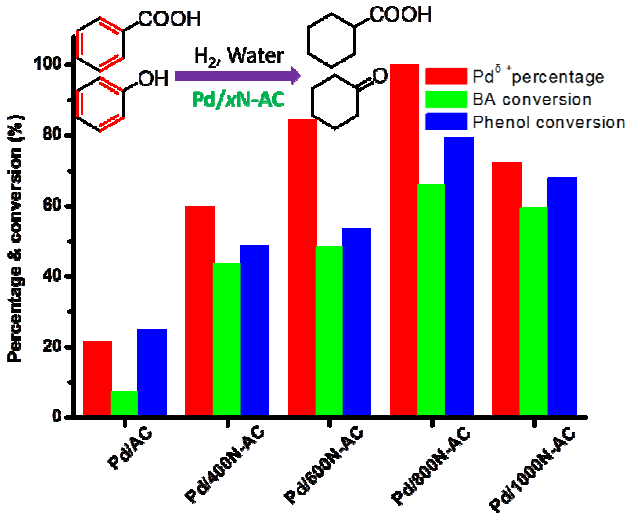

Pyridinic nitrogen species in N-doped active carbon (*x*N-AC) are responsible for high activity of ring hydrogenation *via* the formation of high percentage of electron-deficient Pd clusters.